Manipulation of Majorana zero modes in double quantum dots

Jesus D. Cifuentes[1] and Luis G. G. V. Dias da Silva[1]

[1] *Instituto de Física, Universidade de São Paulo, C.P. 66318, 05315–970 São Paulo, SP, Brazil*

(Dated: February 13, 2019)

Luis *We'll call them Majorana "zero modes" instead of "Majorana fermions", which relates more to elementary particles.* Jesus *Ok ;)*

Majorana zero modes (MZMs) appearing at the edges of topological superconducting wires are a promising platform for fault-tolerant quantum computation. Novel proposals use MZMs tunneling inside quantum dots (QDs) to implement quantum architectures because todays precise experimental control over the QD parameters offers the unique possibility of manipulating the Majoranas inside multi-dot systems. The simplest case where Majorana manipulation is possible is in a double quantum dot (DQD). This model shows several possibilities for manipulation of MZM, including different geometric couplings such as linear forms of T-junctions. In this model we perform analytical (non-interacting) and numerical(interacting) quantum transport studies of the transition of the Majorana signature. By tuning the model parameters we show that it is possible to control the localization of the MZM inside the DQD.

I. INTRODUCTION

→ *Majorana zero modes in condensed matter systems: they have been found, several papers have been written about it and there has been much progress in distinguishing them from other sources of zero-bias peaks.*

The pursuit of Majorana quasi-particles in topological superconductors has attracted significant attention in the last decades.[1,2] Since the first Kitaev's toy models[3,4] claiming promising applications to quantum computing, the field evolved rapidly towards physical realizations of the Kitaev chain. The last few decades have been full of excitement as new technological innovations allowed to document several times the observation of Majorana signatures.[5–10] One of the most promising structures is the so-called Majorana wire, which recipe consists in growing semiconducting wires with strong-orbit-coupling over proximity-induced topological (p-wave) superconductors.

These signatures are characterized by the emergence of robust zero modes localized at the edges of the material. However the observed Majorana zero-modes (MZM) have been found in superposition with other similar types of phenomenon such as Andreev bound states[11] the Kondo effect,[12] which generates certain skepticism regarding the observed Majorana signatures. This conundrum could be solves either by engineering methods to separate the MZM from the other effects[13,14], or by measuring non-abelian statics on braiding protocols,[15–17], a basic operation for topological quantum computing. Current research in this field is focused on these directions.

→ *MZMs in quantum dots can co-exist with Kondo peaks.*

One of the most promising methods to detect MZMs consists in attaching a quantum dot (QD) to the edges of a Majorana chain in the topological phase and executing transport measurements through the QD.[18] In such arrangement the MZM at the end of the chain leaks inside the ,QD[19] which produces a zero-bias conductance peak of half a quanta $\frac{e^2}{2h}$ through the dot. Recent experiments including hybrid Majorana-QD systems[9,20] have increase the expectations on this method which could bring the following advantages: 1) The qubit information is not completely destroyed, in contrast to other detection methods such as tunneling spectroscopy. 2) If performed under the Kondo temperature T_k, it allows to observe the co-existance of the MZM with Kondo effect.[21,22] We showed in a previous project that it is possible to separate both effects by inducing a Zeeman magnetic field to quench the Kondo effect.[13] 3) Todays precise experimental control over the QD parameters allows the manipulation of the MZMs inside multi-dot systems. Hence bringing new lights into the design of scalable quantum architectures.[23,24]

Luis *Ok. Ref. 24 is PRB of scalable designs: PRB* ***95*** *235305 (2017).*

→ *Here's what we did: quantum tunneling of a MZM into a double dot shows several possibilities for manipulation of MZM*

The simplest case where Majorana manipulation is possible is in a double quantum dot (DQD). Tunneling Majorana modes in these basic structures have inspired theoretical studies[25,26] and experimental setups confirming the observations of Andreev molecules[20]. However, there is still no complete analysis of the transitions of the Majorana signatures between the QDs in this model. In this paper we fill this gap by performing a transport study of a DQD coupled to a MZM and a metallic lead FIG.1). We observed that quantum tunneling of a MZM into a double dot shows several possibilities for MZM manipulation. The simplicity of our model allows us to explore many of these alternatives analytically taking into account different geometries of the QD's, from symmetric and linear couplings to T-junctions (FIG.2).In addition, we considered both non-interacting and interacting regimes, observing major agreement between both approaches concerning the location of the Majorana signature. While the non-interacting regime is suitable to

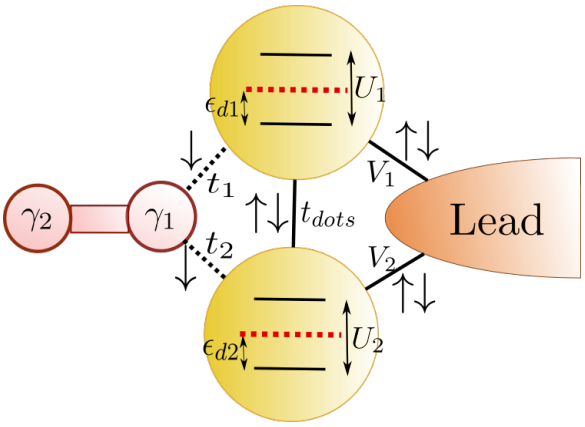

FIG. 1: Model for the DQD-Majorana system. Solid lines: Hopping interactions (t_{dots}: inter-dot coupling , V_1, V_2 couplings of QD1 and QD2 with the lead.). Dashed lines: Majorana spin-↓ effective couplings (6) t_1, t_2. The atomic energy levels appear inside each QD ϵ_1, ϵ_2 are tuned by the gate voltages. The coulomb interaction is represented by U_1, U_2. The red dashed horizontal lines represent the Fermi level.

obtain exact expressions for the Green function, the interacting case shows the Majorana signature co-existing with strongly correlated phenomena such as the Kondo effect[27] and RKKY interactions.[28–30]

This paper is organized as follows. In II we describe our model of a DQD coupled to a MZM and a metalic lead . This model is studied through the ballistic transport[31] approach (non-interacting) in II B and the numerical renormalization group (NRG)[32] in the interacting case II C. The results are presented in section III where we compare the non-interacting density of states (DOS) III A with the low-energy interacting results III B.

II. MODEL AND METHODS

We consider the setup shown in Figure 1 in which an MZM at the edge of Topological Superconductor(TS) is coupled to a double quantum dot (DQD) attached to a single metallic lead. The Hamiltonian of this system can be partitioned in four terms: the DQD Hamiltonian H_{DQD} , the Lead Hamiltonian H_{Lead} , the DQD-lead interaction $H_{DQD-Lead}$ and the coupling between the DQD and the Majorana mode H_{M-DQDs} and

$$H = H_{DQD} + H_{Lead} + H_{DQD-Lead} + H_{M-DQD} \quad (1)$$

The interacting Anderson Model describes the DQD-lead system

$$H_{DQD} = \sum_{i\in\{1,2\}} \sum_{\sigma\in\{\downarrow,\uparrow\}} \left(\epsilon_{di} + \frac{U_i}{2}\right) \hat{n}_{i\sigma} + \frac{U_i}{2}(\sum_{\sigma} \hat{n}_{i\sigma} - 1)^2 + \sum_{\sigma\in\{\uparrow,\downarrow\}} t_{dots}(d^\dagger_{1\sigma} d_{2\sigma} + d^\dagger_{2\sigma} d_{1\sigma}), \quad (2)$$

and

$$H_{Lead} = \sum_{\mathbf{k}\sigma} \epsilon_{\mathbf{k}} c^\dagger_{\mathbf{k}\sigma} c_{\mathbf{k}\sigma} \quad (3)$$

$$H_{DQD-Lead} = \sum_{\mathbf{k}\sigma} \sum_{i\in\{1,2\}} V_{i\mathbf{k}} c^\dagger_{\mathbf{k}\sigma} d_{i\sigma} + V^*_{i\mathbf{k}} d^\dagger_{i\sigma} c_{\mathbf{k}\sigma}, \quad (4)$$

where ϵ_{di} is the energy level of dot i, U_i is the Coulomb repulsion and t_{dots} is the coupling parameter between both QDs. The operator $d^\dagger_{i\sigma}$ creates a particle in dot i with spin σ and $\hat{n}_{i\sigma} := d^\dagger_{i\sigma} d_{i\sigma}$ is the particle number operator of state i. $c^\dagger_{\mathbf{k}\sigma}$ is the creation operator a particle with momentum $\mathbf{k}$ and spin σ in the lead. $\epsilon_{\mathbf{k}l}$ is the corresponding energy and $V_i(\mathbf{k})$ describes the tunneling coupling between the lead and dot i .

The Majorana modes are modeled as a superposition of the creation and annihilation operators of a spin ↓ particle $f_\downarrow$

$$\gamma_1 := \frac{1}{\sqrt{2}}\left(f^\dagger_\downarrow + f_\downarrow\right), \gamma_2 := \frac{i}{\sqrt{2}}\left(f^\dagger_\downarrow - f_\downarrow\right). \quad (5)$$

This makes possible to define an effective coupling between the Majorana Mode and the DQD by attaching γ_1 with the spin-↓ channel in the QDs

$$H_{M-DQD} = \sum_{i=1}^{2} t_i \left(d^\dagger_{i\downarrow}\gamma_1 + \gamma_1 d_{i\downarrow}\right) + \epsilon_M \gamma_1 \gamma_2. \quad (6)$$

where t_i is the coupling parameter between the Majorana mode and QD i. ϵ_m is the coupling energy between both Majorana modes.

A. Methods

B. Non-interacting system

Using Zubarev's ballistic transport approach[31], we derived an exact expression for the Green functions associated to both quantum dot operators $(G_{d_1 d_1^\dagger}(\omega), G_{d_2 d_2^\dagger}(\omega))$. The detailed procedure is included in Appendix A. The transport equations define a 9×9 linear system where the Hamiltonian parameters $(t_1, t_2, \epsilon_1 \ldots)$ and the energy ω are taken as algebraic variables. The solution of this type of equations is a polynomial fraction of the same degree which makes

difficult to provide an exact solution using analytical or numerical methods. To bypass this problem, we associated this transport system to a flow graph and executed a Graph-Gauss-Jordan elimination process[33]. This method proofed to be efficient to solve complex transport systems since the graph structure allows us to identify minimum cutting points and create an algorithmic representation of the Green function.

At the end, we obtained the following analytical expression

$$G_{d_{1\downarrow},d^{\dagger}_{1\downarrow}}(\omega) = \frac{1}{\omega - \epsilon^{+}_{DQD} - \frac{\|T_+\|^2}{\omega-\epsilon_{M2}-\frac{\|T_-\|^2}{\epsilon^{-}_{DQD}}}}. \quad (7)$$

Where

$$\epsilon^{\pm}_{DQD} = \pm\epsilon_1 + \sum_{\mathbf{k}} \frac{V_1 V_1^*}{\omega-\epsilon_{\mathbf{k}}} + \frac{\left\|\pm t_{dots} + \sum_{\mathbf{k}} \frac{V_1 V_2^*}{\omega-\epsilon_{\mathbf{k}}}\right\|^2}{\omega \pm \epsilon_2 - \sum_{\mathbf{k}} \frac{V_2 V_2^*}{\omega-\epsilon_{\mathbf{k}}}}, \quad (8)$$

$$T_{\pm} = \pm t_1 \pm t_2 \frac{\left(\pm t_{dots} + \sum_{\mathbf{k}} \frac{V_1 V_2^*}{\omega-\epsilon_{\mathbf{k}}}\right)}{\omega \pm \epsilon_2 \pm \sum_{\mathbf{k}} \frac{V_2 V_2^*}{\omega-\epsilon_{\mathbf{k}}}}, \quad (9)$$

and

$$\epsilon_{M2} = \omega - \epsilon_M - \frac{\frac{\omega}{\omega+\epsilon_M}\|t_2\|^2}{\omega - \epsilon_2 - \sum_{\mathbf{k}} \frac{V_2 V_2^*}{\omega-\epsilon_{\mathbf{k}}}} - \frac{\frac{\omega}{\omega+\epsilon_M}\|t_2\|^2}{\omega + \epsilon_2 - \sum_{\mathbf{k}} \frac{V_2 V_2^*}{\omega+\epsilon_{\mathbf{k}}}}. \quad (10)$$

On the other hand the spin-↑ DOS, which is not coupled to the MZM, can be obtained by taking $t_1, t_2 = 0$, hence giving

$$G_{d_{1\uparrow},d^{\dagger}_{1\uparrow}}(\omega) = \frac{1}{\omega - \epsilon^{+}_{DQD}}. \quad (11)$$

The final results will depend on the broadening parameter of QD i with the lead (Γ_i). This broadening satisfies the equation

$$-i\Gamma_i = \lim_{s\to 0} \sum_{\boldsymbol{k}} \frac{V_i^* V_i}{\omega + is - \epsilon_{\boldsymbol{k}}}. \quad (12)$$

By convention we take Γ_1 as the energy unit for the rest of the project. Finally we compute the DOS

$$\rho_{1\sigma}(\omega) = -\frac{1}{\pi}\mathrm{Im}\left[G_{d_{1\sigma},d^{\dagger}_{1\sigma}}(\omega))\right]. \quad (13)$$

Similar results can be obtain for the DOS of the second $\rho_{2\sigma}$ by exchanging the indexes 1 and 2 in equation (11).

The density of states provides significant information about the presence of a Majorana zero modes in the dot. We characterize the Majorana signature by a robust zero-mode with two possible heights:

- **Type I:** The spin-↓ DOS is the half of the spin-↑ DOS at the Fermi energy ($\rho_\downarrow(0) = \rho_\uparrow(0)$).
- **Type II:** A spin-↓ zero mode of height $\rho_\downarrow(0) = \frac{0.5}{\pi\Gamma_1}$.

In our results we observe several times these two types of signatures. Type I often appears when there is a zero-mode in the spin-↑ DOS. Type II emerges in the other situations.

C. Interacting case (NRG)

The Numerical Renormalization Group (NRG)[32,34,35] is the most successful methods to study interacting quantum impurity models. In this model, the impurity is described by the DQD attached to the MZM. In our code, we set a Coulomb repulsion factor of $U = 17.3\Gamma_1$ in both dots and a cut-off energy of $D = 2U = 34.6\Gamma_1$. The spacing with other energy levels is assumed to be higher than D, such that only the two coulomb states are relevant for the system dynamics. When $\epsilon_i = \frac{U}{2}$ in both dots, the system is in the Particle-Hole-Symmetric region. At this point, each dot has an odd number of electrons, hence, at sufficiently low temperature the system will exhibit the characteristic Kondo peaks at the Fermi energy Wilson[34]. The coexistence of Kondo and Majorana zero modes is still a point of contention in the area and one of the objectives of this part of the project

To improve the efficiency of the code we used the symmetries of the system to maintain a block structure during NRG's iterative diagonalization process. This model preserves the spin-↑ particle number $\hat{N}_\uparrow$ and the spin-↓ parity $\hat{P}_\downarrow = \pm$ (+ even, − odd). The spin-↓ particle number is not preserved due to superconducting-type Majorana coupling (6) . The initial Hamiltonian is organized in blocks according to these symmetries. This block structure is preserved during the entire iteration process[32]. To compute the spectral functions, we use the density matrix renormalization group (DM-NRG)[36] in combination with the Z-trick method[37], which improves the spectral resolution at high energies.

III. RESULTS

We call MZM manipulation to the "movements" attributed to the Majorana signature under the tunning of the dot gate voltages (ϵ_1, ϵ_2). This manipulation process is performed in three different set ups that are presented in 2 with definite values of Γ_2, t_dots, t_1 and t_2. In configuration (a), we coupled the QD symmetrically to the lead and the Majorana mode. With this setup we expect to break the localization of the MZM which should split and tunnel into both dots. In setups (b) and (c) we coupled the second dot indirectly through the first dot. Hence, quantum interference should split the zero mode in two states. Our objective is to observe what occurs with the Majorana signature in this situation. There are two options to connect the MZM in this situation. Attached it

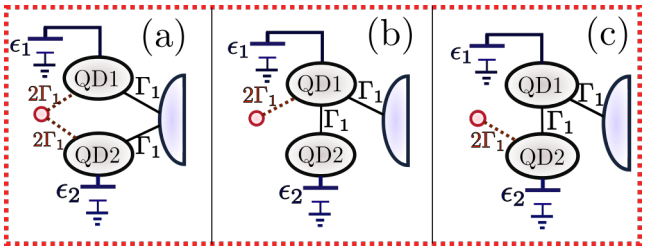

FIG. 2: Cases of study: (a) Symmetric coupling of the DQD to the lead and the MZM. No inter-dot coupling. (b)&(c) Indirect coupling of the second QD through the first dot. The Majorana is coupled to the (b) first dot or to the (c) second dot.

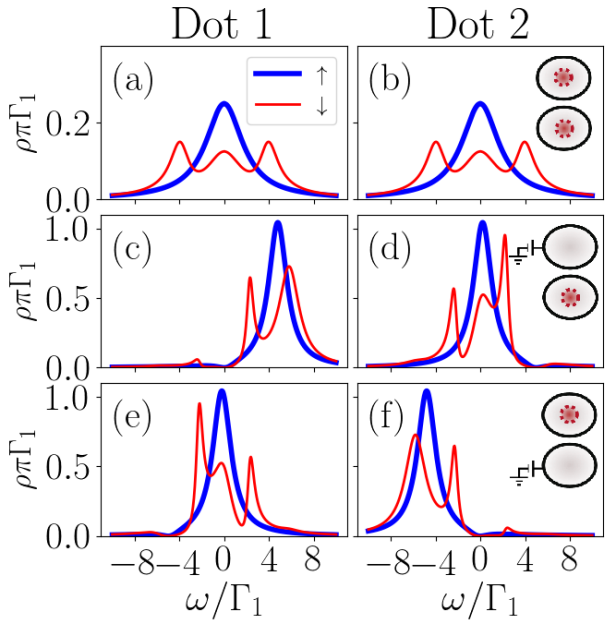

FIG. 3: Non-interacting DOS in the symmetric coupling setup (FIG.2(a)) at each QD. First column: Dot 1. Second column: Dot 2. The gate voltages vary at each row. First row: Zero gate voltages $\epsilon_1 = \epsilon_2 = 0$. Second row: $\epsilon_1 = 5\Gamma_1$, $\epsilon_2 = 0$. Third row: $\epsilon_1 = 0$, $\epsilon_2 = -5\Gamma_1$. Bold blue lines: Spin-↑ DOS. Thin red lines: Spin-↓ DOS. The insets at the right show which dot carries a Majorana signature, represented by a red dashed circle. Upper: First dot. Lower: Second dot.

directly through the first dot (b) or indirectly through the second dot (c). Both alternatives are geometrically distinct since (b) suggests a T-junction coupling while (c) reflects a connection in series of both QD's between the lead and the MZM.

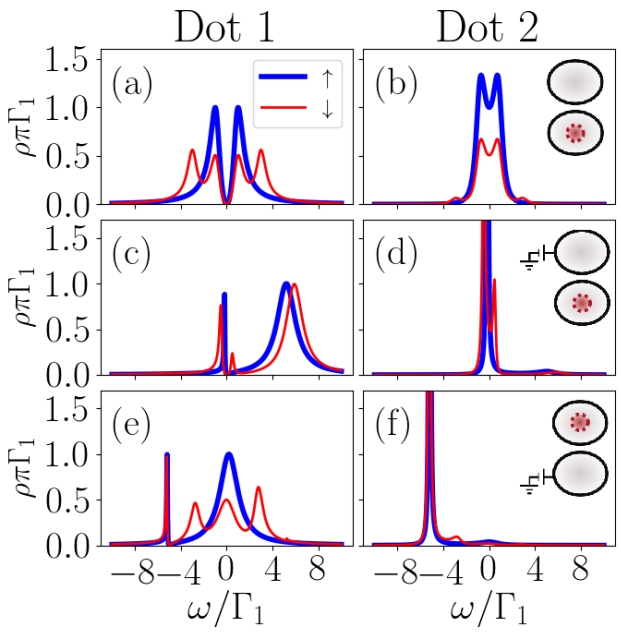

FIG. 4: The same as in FIG.3 for the non-interacting DOS of the setup in FIG.2(b)

A. MZM manipulation in non-interacting quantum dots

The non-interacting results for setups (a),(b) and (c) of 2 are shown at figures 3, 4 and 5 respectively. Each figure depicts the DOS of dot 1(left) and dot 2(right). The gate voltage is initially 0 in both dots at the first row. In the second row, the gate voltage is turned on to $\epsilon_1 = 5\Gamma_1$, while the second dot remains at $\epsilon_2 = 0$. In the third row the first dot's voltage is off $\epsilon_1 = 0$ and we switch on the second dot with a negative voltage of $\epsilon_2 = -5\Gamma_1$. The inset figures at the right side of each row show which dots exhibit Majorana signatures, depicted by a red dashed circle inside the dot. These images will continuously change under the tuning of gate voltages which represents the manipulation of the Majorana signature.

In FIG.3 we observe the results for the symmetric coupling setup FIG.2(a). In the particle hole symmetric case (first row) the DOS is equal in both dots. Note that that the spin-↓ (Thin red line) DOS is the half of the spin-↑ (Bold blue line) DOS at the Fermi energy ($\rho_\downarrow(0) = \frac{1}{2}\rho_\uparrow(0)$). This type II Majorana signature is similar to the one observed when a single dot is coupled to a Majorana mode.[18] We may conclude that the Majorana in tunneling inside both dots breaking the localization of the MZM. If a positive or negative gate voltage is induced in one of the dots, as shown in the second and third row of Figure 3(c)-(f), the Majorana zero mode vanishes from that dot. Meanwhile the density of states in the other dot increases while preserving the Majorana signature. This means that the MZM is actually being in-

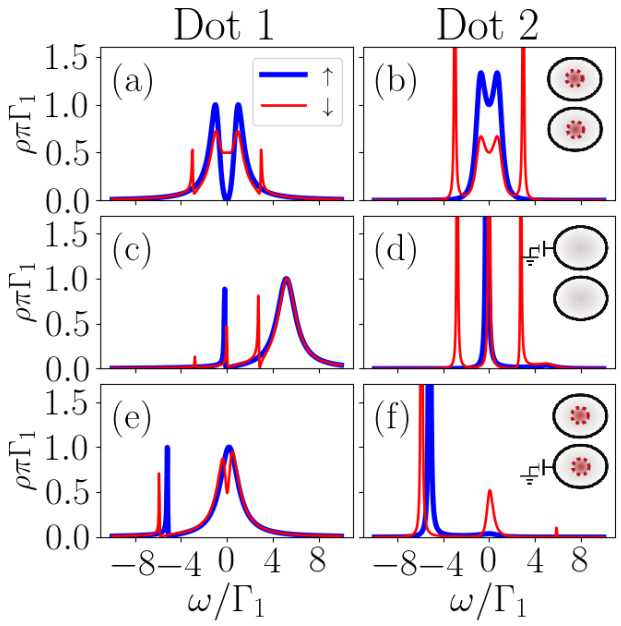

FIG. 5: The same as in FIG.3 for the non-interacting DOS of the set up in FIG.2(c) .

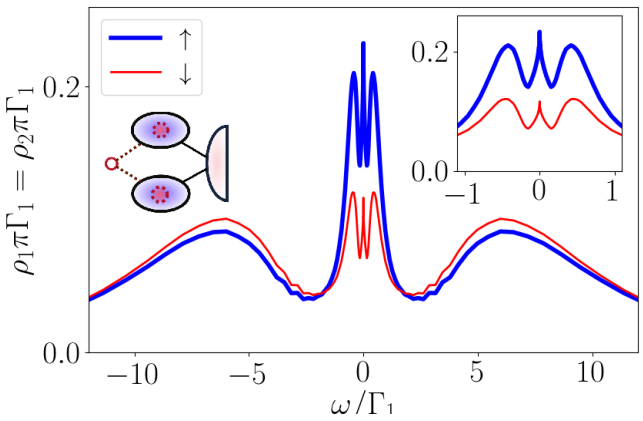

FIG. 6: Density of states of both dots in the symmetric coupling without gate voltages between the Majorana and the interacting DQD. Bold blue lines: Spin-↑ DOS. Thin red lines: Spin-↓ DOS. Inset: Low-energy DOS.

duced to "leave" this dots and leak into the other dot by the gate voltage activation. This first example of MZM manipulation.

Another example of MZM manipulation occurs when the second dot is not directly connected to the lead. In this case, the inter-dot tunneling generates quantum interference which finally destroys the central peak as observe in FIG.4(a) at the spin-↑ DOS . The spin-↓ channel at FIG.4(a), which is coupled to the MZM, does not exhibit the characteristic Fermi peak either. Instead, the one half Majorana signature at the Fermi energy ($\rho_\downarrow(0) = \frac{1}{2}\rho_\uparrow(0)$) appears clearly inside the second dot FIG.4(b). This situation prevails when the first dot's gate voltage is turned on FIG.4(c)&(d). While the first dot does not seem to exhibit any type of Majorana signature, the second dot's spin-↓ DOS exhibits a robust zero-mode of height $\frac{0.5}{\pi\Gamma}$. The results are more exciting when the second dot's gate voltage is turned on in FIG.4(e)&(f). These figures clearly show how the MZM, previously localized at the second dot, is induced to leave this dot and returned onto the first dot. Moreover, the DOS of spin-↑ and spin-↓ channels are very similar to the spectral densities observed at FIG.3(d)(e), which means that the previous interference pattern has disappeared due to the presence of this gate voltage.

The results of the third configuration FIG.2(c) appear in FIG.5. Contrary to what was observed in the previous case, this time the Majorana signature is not destroyed by the interference but instead, the $\frac{0.5}{\pi\Gamma}$-height MZM emerges indirectly in the first dot. This is a perfect way to separate the Majorana's spin-↓ DOS from the central spin-↑ zero-mode which is still destroyed by the interference. In addition, the second dot still exhibits a type I Majorana signature as observed in FIG.5(b). In the second row we observe that turning on the gate voltage in dot 1 destroys the Majorana signature in both dots FIG.5(c)(d). On the other hand, if the second dot's voltage is switched both dots will preserve their Majorana signature (QD1:type I, QD2: type II), while the spin-↑ quantum interference vanishes in the first dot.

B. MZM manipulation in interacting dots

Now we consider a Coulomb repulsion energy of $U = 17\Gamma_1$ in both dots. The factor $\frac{U_i}{2}(\sum_\sigma \hat{n}_{i\sigma} - 1)^2$ in (2) favors states with an odd number of electrons (and holes). In addition, particle-hole equilibrium is now achieved when $\left(\epsilon_{di} + \frac{U_i}{2}\right)\hat{n}_{i\sigma}$. Any induced gate voltage must be considered as a shifting from this equilibrium point. FIG6 shows the DOS at both QDs for the symmetric coupling configuration 2. The two peaks appearing at around $8.6\Gamma_1 = \frac{U_i}{2}$ represent the two energy levels spaced by the Coulomb repulsion factor U. The central spin-↑ peak is a consequence of the Kondo effect,[27,34] while the two satellite peaks observed in the inset are the result of the RKKY indirect interaction between both dots.[28–30] Moreover, the system presents a Majorana signature characterized by half spin-↓ DOS at the Fermi energy ($\rho_\downarrow(0) = \frac{1}{2}\rho_\uparrow(0)$) . Note, that in this case the Majorana signature coexists with the Kondo effect in the DQD as already predicted by Ruiz-Tijerina *et al.* for a single dot.[13]

In this part of the project we are interested in the physics at low energy scales $\omega \sim \Gamma_1$ inside the gap form by the Coulomb peaks as in the inset of FIG.6. Is at this region where the Kondo and Majorana peaks are observable . At this scale the results are comparable with the non-interacting case. For instance, FIG.7 shows

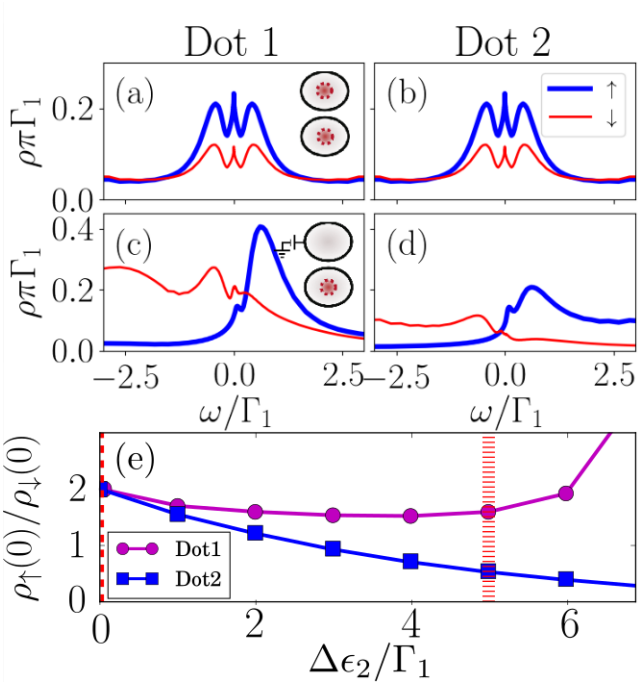

FIG. 7: The same as in FIG.3 for the interacting DOS in the symmetric coupling (FIG.2(a)). (e): Evolution of $\frac{\rho_\downarrow(0)}{\rho_\uparrow(0)}$ vs increasing gate voltage $\Delta\epsilon_2$. Dash line: $\epsilon_2 = 0$ as in (a),(b). Bar line: $\epsilon_2 = 5\Gamma_1$ as in (c),(d).

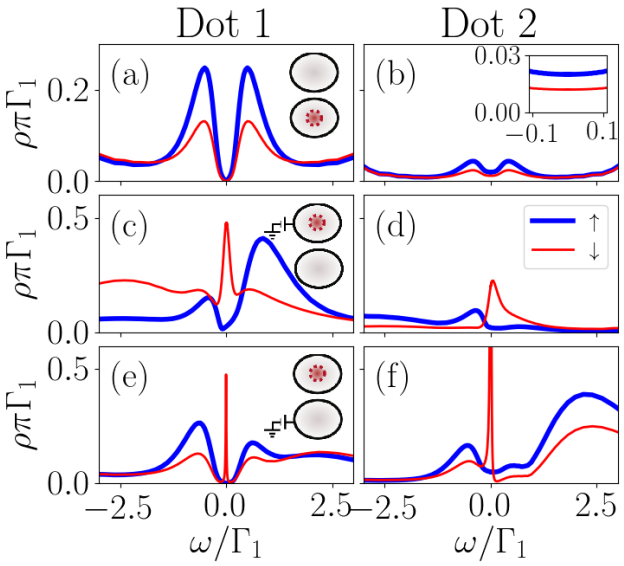

FIG. 8: The same as in FIG.3 for the interacting DOS of the setup in FIG.2(b). Inset in b): Low-energy DOS.

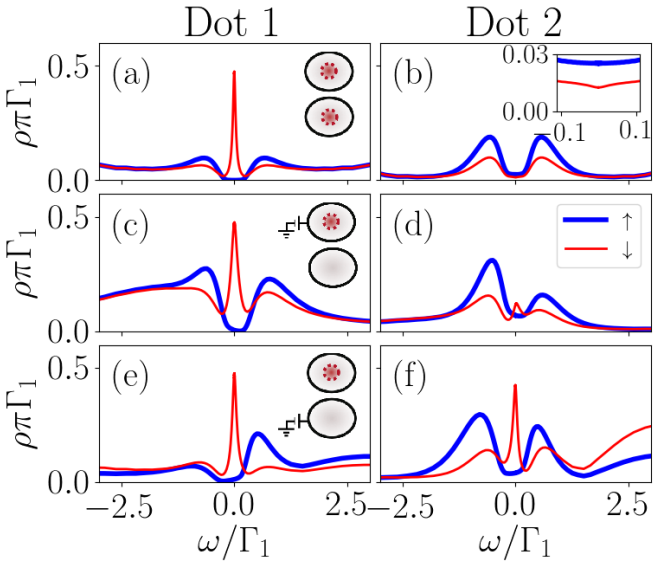

FIG. 9: The same as in FIG.3 for the interacting DOS of the set up in FIG.2(c) . Inset in b): Low-energy DOS.

the NRG results for the symmetric setup in FIG.2(a). In agreement with the non-interacting results, both dots have type I Majorana signatures. These signatures can be manipulated by tuning one of the dot's gate voltage to induce the MZM to leak into the other dot. The DOS at figures FIG.7(d) shows a type I Majorana signature with $\rho_\downarrow(0) \approx \frac{1}{2}\rho_\uparrow(0)$). This Majorana signature is stable for adjustments of energies bellow the $6\Gamma_1$ (see FIG.7(e)). At larger gate voltages the coulomb peak at $\omega \sim 8.7$ overlaps with the Fermi energy which destroys both signals.

In the second setup FIG.2(b), the spin-↑ Kondo peak in FIG.8 is destroyed by interference just as in the non-interacting case. This phenomenon had already been predicted for a T-junction of a double quantum dot attached to metallic leads[38]. The insight of our model is that an attached MZM should also disappear due to the same interference. Furthermore, a type I Majorana signature can be observed at very low energies in the inset of FIG.8(b). However we have to recognize that both zero-modes decay significantly in the second dot. When the first voltage is turned on, the Majorana mode jumps onto the first dot which presents a type I Majorana signature. This is a clear difference with the non-interacting results where the Majorana signature stayed in the second dot. If the second dot is switched on , a type II Majorana signature appears a very low energies in dot 1, which is coherent with the idea that the Majorana interference should disappear in this case. In FIG.8(e) we identify the emergy of a Fano resonance at the Fermi energy causing the sharp-asymmetric peak at $\omega = 0$.

Finally, FIG.9 depicts the NRG results for the last configuration FIG.2(c). Surprisingly, the indirectly-attached MZM exhibits a robust type II Majorana signature in the first dot over a destroyed Kondo peak. This signature is stable under the gate voltage tuning. In addition, only in the particle hole symmetric case the second dot presents a type II Majorana signature (Inset FIG.9(b)). We could understand this effect by thinking that the QDs in model (c) are attached in series. Therefore the two dots can

be thought as extensions of the Kitaev chain being the first dot the last place in the wire. Hence the Majorana should be localized at this dot despite the application of gate voltages. This case is similar to the case of a single dot attached to a Majorana chain, where it is known that the MZM appears in the dot even when this is supposed to be empty[19]. It still remains the doubt about why this effect is not observed in the non-interacting case . On the other hand, there is a significant zero-mode in the spin-↓ DOS. This mode was not identified as a potential Majorana signature since it increases when $\delta\epsilon_2$.

IV. CONCLUDING REMARKS

Comparing the exact analytical solution in the non-interacting system and the NRG results for interacting quantum dots, we were able to characterized the displacements of the MZM inside the double quantum dot for the three setups in FIG.2. We observe a considerable agreement on the location of the Majorana signature between the interacting and non-interacting results:

FIG.2(a): In the symmetric coupling the MZM leaks inside both dots. For interacting dots, the Majorana signature will be distinguishable near the Kondo temperature. At this regime the system presents combined Kondo-Majorana physics . If the gate voltage of one dot is turned on the MZM is induced to tunnel only into the other dot.

FIG.2(b): In this system the spin-↑ zero mode at QD1 (The Kondo peak if the system is interacting) is destroyed by quantum interference with the second dot. This interference will also destroy the MZM in the first dot but a type I Majorana signature will still appear in the second dot. The Majorana mode can be induced to tunnel back into the first dot if a gate voltage is applied on the second dot. This signature is visible at very low energies (bellow $0.1\Gamma_1$) in interacting case.

FIG.2(c): An indirect type II Majorana signature is observed in the first dot. This signature is robust, specially in the interacting case, where it is present in all configurations.

ACKNOWLEDGMENTS

The authors thank Edson Vernek for enlightening discussions. L.G.G.V.D.S. acknowledges financial support by CNPq (grants No. 307107/2013-2 and 449148/2014-9), and FAPESP (grant No. 2016/18495-4).

[1] J. Alicea, Reports on Progress in Physics **75**, 076501 (2012).
[2] C. Beenakker, Annual Review of Condensed Matter Physics **4**, 113 (2013).
[3] A. Y. Kitaev, Physics-Uspekhi **44**, 131 (2001).
[4] A. Y. Kitaev, Annals of Physics **303**, 2 (2003), arXiv: quant-ph/9707021.
[5] V. Mourik, K. Zuo, S. M. Frolov, S. R. Plissard, E. P. a. M. Bakkers, and L. P. Kouwenhoven, Science **336**, 1003 (2012).
[6] A. Das, Y. Ronen, Y. Most, Y. Oreg, M. Heiblum, and H. Shtrikman, Nature Physics **8**, 887 (2012).
[7] M. T. Deng, C. L. Yu, G. Y. Huang, M. Larsson, P. Caroff, and H. Q. Xu, Nano Letters **12**, 6414 (2012).
[8] S. Nadj-Perge, I. K. Drozdov, J. Li, H. Chen, S. Jeon, J. Seo, A. H. MacDonald, B. A. Bernevig, and A. Yazdani, Science **346**, 602 (2014).
[9] M. T. Deng, S. Vaitiekenas, E. B. Hansen, J. Danon, M. Leijnse, K. Flensberg, J. Nygard, P. Krogstrup, and C. M. Marcus, Science **354**, 1557 (2016).
[10] H. Zhang, C.-X. Liu, S. Gazibegovic, D. Xu, J. A. Logan, G. Wang, N. van Loo, J. D. S. Bommer, M. W. A. de Moor, D. Car, R. L. M. Op het Veld, P. J. van Veldhoven, S. Koelling, M. A. Verheijen, M. Pendharkar, D. J. Pennachio, B. Shojaei, J. S. Lee, C. J. Palmstrm, E. P. A. M. Bakkers, S. D. Sarma, and L. P. Kouwenhoven, Nature **556**, 74 (2018).
[11] S. D. Sarma, J. D. Sau, and T. D. Stanescu, Physical Review B **86** (2012), 10.1103/PhysRevB.86.220506, arXiv: 1211.0539.
[12] E. J. H. Lee, X. Jiang, R. Aguado, G. Katsaros, C. M. Lieber, and S. De Franceschi, Physical Review Letters **109**, 186802 (2012).
[13] D. A. Ruiz-Tijerina, E. Vernek, L. G. G. V. Dias da Silva, and J. C. Egues, Physical Review B **91**, 115435 (2015).
[14] C.-X. Liu, J. D. Sau, T. D. Stanescu, and S. Das Sarma, Physical Review B **96**, 075161 (2017).
[15] D. Aasen, M. Hell, R. V. Mishmash, A. Higginbotham, J. Danon, M. Leijnse, T. S. Jespersen, J. A. Folk, C. M. Marcus, K. Flensberg, and J. Alicea, Physical Review X **6**, 031016 (2016).
[16] S. D. Sarma, M. Freedman, and C. Nayak, npj Quantum Information **1**, 15001 (2015).
[17] B. v. Heck, A. R. Akhmerov, F. Hassler, M. Burrello, and C. W. J. Beenakker, New Journal of Physics **14**, 035019 (2012).
[18] D. E. Liu and H. U. Baranger, Physical Review B **84** (2011), 10.1103/PhysRevB.84.201308, arXiv: 1107.4338.
[19] E. Vernek, P. H. Penteado, A. C. Seridonio, and J. C. Egues, Physical Review B **89**, 165314 (2014).
[20] Z. Su, A. B. Tacla, M. Hocevar, D. Car, S. R. Plissard, E. P. A. M. Bakkers, A. J. Daley, D. Pekker, and S. M. Frolov, Nature Communications **8**, 585 (2017).
[21] M. Lee, J. S. Lim, and R. Lopez, Physical Review B **87**, 241402 (2013).
[22] G. Grski, J. Baraski, I. Weymann, and T. Domaski, Scientific Reports **8**, 15717 (2018).
[23] M. Barkeshli and J. D. Sau, arXiv:1509.07135 [cond-mat, physics:quant-ph] (2015), arXiv: 1509.07135.
[24] T. Karzig, C. Knapp, R. M. Lutchyn, P. Bonderson, M. B.

Hastings, C. Nayak, J. Alicea, K. Flensberg, S. Plugge, Y. Oreg, C. M. Marcus, and M. H. Freedman, Physical Review B **95**, 235305 (2017).
[25] J. F. Silva and E. Vernek, Journal of Physics: Condensed Matter **28**, 435702 (2016).
[26] T. I. Ivanov, Physical Review B **96**, 035417 (2017).
[27] A. C. Hewson, *The Kondo Problem to Heavy Fermions* (Cambridge University Press, 1997) google-Books-ID: fPzgHneNFDAC.
[28] M. A. Ruderman and C. Kittel, Physical Review **96**, 99 (1954).
[29] T. Kasuya, Progress of Theoretical Physics **16**, 45 (1956).
[30] K. Yosida, Physical Review **106**, 893 (1957).
[31] D. N. Zubarev, Soviet Physics Uspekhi **3**, 320 (1960).
[32] R. Bulla, T. A. Costi, and T. Pruschke, Reviews of Modern Physics **80**, 395 (2008).
[33] D. A. Spielman, *Algorithms, Graph Theory, and Linear Equations in Laplacian Matrices*, Proceedings of the International Congress of Mathematicians (2010).
[34] K. G. Wilson, Reviews of Modern Physics **47**, 773 (1975).
[35] M. Sindel, *Numerical Renormalization Group studies of Quantum Impurity Models in the Strong Coupling Limit*, Text.PhDThesis, Ludwig-Maximilians-Universitt Mnchen (2005).
[36] W. Hofstetter, Physical Review Letters **85**, 1508 (2000).
[37] W. C. Oliveira and L. N. Oliveira, Physical Review B **49**, 11986 (1994).
[38] L. G. G. V. Dias da Silva, N. Sandler, K. Ingersent, and S. E. Ulloa, Physica E: Low-dimensional Systems and Nanostructures **40**, 1002 (2008).

Appendix A: Computation of the Green Function

In Zubarev's fermionic ballistic transport approach[31] the green function associated to two operators $A(t)$, $B(t)$ is defined as that Fourier transform of the time-ordered anti-commutator of A and B

$$G_{A,B}(\omega) = \mathcal{F}\left\{\mathcal{T}\left[\{A(t), B(t')\}\right]\right\}(\omega)\,. \tag{A1}$$

The Fourier transform of Schrodinger evolution leads to the the transport equations

$$\omega G_{A,B}(\omega) = \delta_{A^\dagger,B} + G_{[A,H],B}(\omega). \tag{A2}$$

Applying this expression to Hamiltonian (1) replacing A and B by the creation and annihilation operators $d\dagger_i, f^\dagger, d_i, f, c_k, c\dagger_k$ we obtain a linear transport system. To simplify the complexity of the equations we fix $B = d^\dagger_{1\downarrow}$. In addition note that if we replace A by $f_\downarrow$ and $f^\dagger_\downarrow$ A2 becomes

$$(\omega - \epsilon_M)\, G_{f_\downarrow, d^\dagger_{1\downarrow}}(\omega) = \frac{t}{\sqrt{2}}\left(G_{d_{1\downarrow}, d^\dagger_{1\downarrow}}(\omega) - G_{d^\dagger_{1\downarrow}, d^\dagger_{1\downarrow}}(\omega)\right) \tag{A3}$$

$$(\omega + \epsilon_M)\, G_{f^\dagger_\downarrow, d^\dagger_{1\downarrow}}(\omega) = \frac{t}{\sqrt{2}}\left(G_{d_{1\downarrow}, d^\dagger_{1\downarrow}}(\omega) - G_{d^\dagger_{1\downarrow}, d^\dagger_{1\downarrow}}(\omega)\right). \tag{A4}$$

This allows us to take $G_{f^\dagger_\downarrow, d^\dagger_{1\downarrow}}(\omega) = \frac{\omega+\epsilon}{\omega-\epsilon} G_{f^\dagger_\downarrow, d^\dagger_{1\downarrow}}(\omega)$. Hence, we can eliminate $G_{f^\dagger_\downarrow, d^\dagger_{1\downarrow}}(\omega)$ from the equations even before we start Gauss-Jordan process.

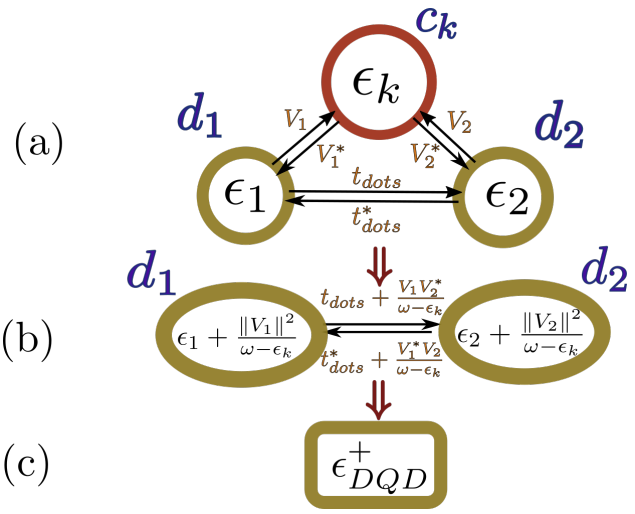

FIG. 10

Writing the other equations we obtain the linear system of the form

$$\mathcal{T}\vec{G}_{d^\dagger_1} = \hat{e_1}, \tag{A5}$$

where $\mathcal{T}$ is the transport matrix

$$\begin{bmatrix}
\omega-\epsilon_1 & -V_1^* & -t_{dots} & \frac{-t_1}{\sqrt{2}} & 0 & 0 & 0 \\
-V_1 & \omega-\epsilon_k & -V_2 & 0 & 0 & 0 & 0 \\
-t^*_{dots} & -V_2^* & \omega-\epsilon_2 & \frac{-t_2}{\sqrt{2}} & 0 & 0 & 0 \\
\frac{-\sqrt{2}t_1^*}{\omega+\epsilon_M} & 0 & \frac{-\sqrt{2}t_2^*}{\omega+\epsilon_M} & \omega-\epsilon_M & \frac{\sqrt{2}t_2^*}{\omega+\epsilon_M} & 0 & \frac{\sqrt{2}t_1^*}{\omega+\epsilon_M} \\
0 & 0 & 0 & \frac{t_2}{\sqrt{2}} & \omega+\epsilon_2 & V_2^* & t^*_{dots} \\
0 & 0 & 0 & 0 & V_2 & \omega+\epsilon_k & V_1 \\
0 & 0 & 0 & \frac{t_1}{\sqrt{2}} & t_{dots} & V_1^* & \omega+\epsilon_1
\end{bmatrix}, \tag{A6}$$

$\vec{G}_{d^\dagger_1}$ is the column vector

$$[G_{d_{1\downarrow}, d^\dagger_{1\downarrow}}(\omega), G_{c_{k\downarrow}, d^\dagger_{1\downarrow}}(\omega), G_{d_{2\downarrow}, d^\dagger_{1\downarrow}}(\omega), G_{f_\downarrow, d^\dagger_{1\downarrow}}(\omega), G_{d^\dagger_{2\downarrow}, d^\dagger_{1\downarrow}}(\omega), G_{c^\dagger_{k\downarrow}, d^\dagger_{1\downarrow}}(\omega), G_{d^\dagger_{1\downarrow}, d^\dagger_{1\downarrow}}(\omega)]^T$$

and $\hat{e_1}$ is the vector with entries $\hat{e}_{1_n} = \delta_{1n}$.

The graph associated to this matrix is the one in FIG.11. The energies inside each vertex are given by subtracting the corresponding diagonal term from ω . The couplings are just the negative of the off-diagonal terms.

1. The double quantum dot

To explain the process of Gaussian elimination we will obtain the green function for the case without Majorana fermion ($t_1 = t_2 = 0$). The transport matrix for this system is

$$\begin{bmatrix}
\omega-\epsilon_1 & -V_1 & -t_{dots} \\
-V_1^* & \omega-\epsilon_k & -V_2 \\
-t^*_{dots} & -V_2^* & \omega-\epsilon_2
\end{bmatrix}. \tag{A7}$$

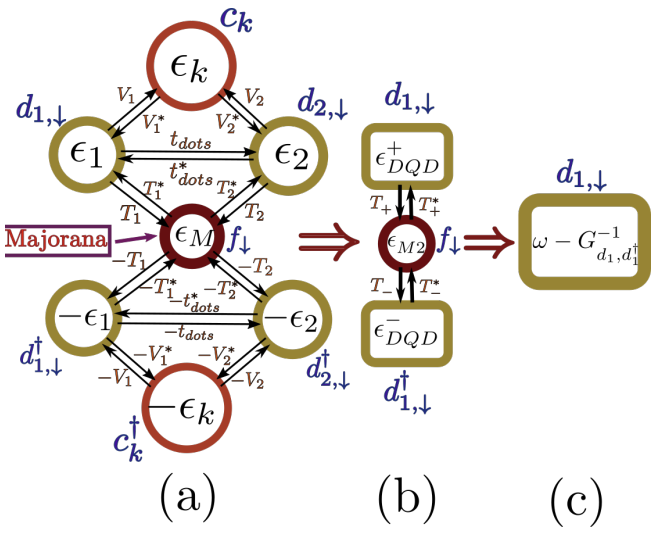

FIG. 11: Transport flow in a DQD Majorana system.

The graph associated to this matrix can be observed in FIG10.a). To eliminate the vertex c_k we just need to subtract from (A7) the rank-1 matrix that cancels the row and the column corresponding to c_k. This matrix is

$$\begin{bmatrix} \frac{V_1^* V_1}{\omega-\epsilon_k} & -V_1^* & \frac{V_2 V_1^*}{\omega-\epsilon_k} \\ -V_1 & \omega-\epsilon_k & -V_2 \\ \frac{V_2^* V_1}{\omega-\epsilon_k} & -V_2^* & \frac{V_2^* V_2}{\omega-\epsilon_k} \end{bmatrix}. \tag{A8}$$

The result of (A7) - (A8) is

$$\begin{bmatrix} \omega-\epsilon_1-\frac{V_1^* V_1}{\omega-\epsilon_k} & 0 & -t_{dots}-\frac{V_2 V_1^*}{\omega-\epsilon_k} \\ 0 & 0 & 0 \\ -t_{dots}^*-\frac{V_2^* V_1}{\omega-\epsilon_k} & 0 & \omega-\epsilon_2-\frac{V_2 V_1^*}{\omega-\epsilon_k} \end{bmatrix} \tag{A9}$$

which is depicted by the graphs in FIG.10.b). The next step is to pop-out the vertex d_2 following the same procedure. At the end, the energy inside the vertex d_1 will be

$$\epsilon_{DQD}^{+} = \epsilon_1 + \sum_{\mathbf{k}} \frac{V_1 V_1^*}{\omega-\epsilon_{\mathbf{k}}} + \frac{\left\| t_{dots} + \sum_{\mathbf{k}} \frac{V_1 V_2^*}{\omega-\epsilon_{\mathbf{k}}} \right\|^2}{\omega-\epsilon_2-\sum_{\mathbf{k}} \frac{V_2 V_2^*}{\omega-\epsilon_{\mathbf{k}}}} \tag{A10}$$

and the green function of $G_{d_1 d_1^\dagger}(\omega)$ in a DQD will be given by $\frac{1}{\omega-\epsilon_{DQD}}$ (see FIG.10.c)).

2. Solution of the transport equations

The previous procedure can be generalized into the following algorithm:

1. Computing the transport equations with the second term fixed in the creation operator of the dot.
2. Setting up the graph associated to the transport system.
3. Popping out the vertexes of the graph. Each popping process carries the following steps.
   (a) Computing the extra-terms in the energies and couplings based on the walks passing through the popped vertex.
   (b) Eliminating this vertex from the graph.
   (c) Iterating till there is only one vertex.
4. The energy in the remaining vertex d is $\epsilon_d = \frac{1}{\omega - G_{d,d^\dagger}(\omega)}$.

Following these steps it is possible to solve the general case. We start with the graph in FIG.11 and we pop out the vertexes $c_k, c_k^\dagger, d_{2,\downarrow}$ and $d_{2,\downarrow}^\dagger$ in that order. The energies associated to $d_{1,\downarrow}$ and $d_{1,\downarrow}^\dagger$ will be similar to (A10) giving

$$\epsilon_{DQD}^{\pm} = \pm\epsilon_1 + \sum_{\mathbf{k}} \frac{V_1 V_1^*}{\omega-\epsilon_{\mathbf{k}}} + \frac{\left\| \pm t_{dots} + \sum_{\mathbf{k}} \frac{V_1 V_2^*}{\omega-\epsilon_{\mathbf{k}}} \right\|^2}{\omega \pm \epsilon_2 - \sum_{\mathbf{k}} \frac{V_2 V_2^*}{\omega-\epsilon_{\mathbf{k}}}}. \tag{A11}$$

There is also a correction in the couplings between the Majorana mode and $d_{1,\downarrow}$, $d_{1,\downarrow}^\dagger$ given by

$$T_{\pm} = \pm t_1 \pm t_2 \frac{\left(\pm t_{dots} + \sum_{\mathbf{k}} \frac{V_1 V_2^*}{\omega-\epsilon_{\mathbf{k}}} \right)}{\omega \pm \epsilon_2 \pm \sum_{\mathbf{k}} \frac{V_2 V_2^*}{\omega-\epsilon_{\mathbf{k}}}}. \tag{A12}$$

Finally since the Majorana is in contact with dot 2, there is an extra-term appearing in the Majorana energy given by

$$\epsilon_{M2} = \omega - \epsilon_M - \frac{\frac{\omega}{\omega+\epsilon_M} \|t_2\|^2}{\omega-\epsilon_2-\sum_{\mathbf{k}} \frac{V_2 V_2^*}{\omega-\epsilon_{\mathbf{k}}}} - \frac{\frac{\omega}{\omega+\epsilon_M} \|t_2\|^2}{\omega+\epsilon_2-\sum_{\mathbf{k}} \frac{V_2 V_2^*}{\omega+\epsilon_{\mathbf{k}}}}. \tag{A13}$$

With all the terms of the graph in FIG.11.b) computed, it only remains to pop out vertexes $d_1^\dagger$ and $f_\downarrow$ in that order to obtain the result in equation (11).

$$G_{d_{1\downarrow}, d_{1\downarrow}^\dagger}(\omega) = \frac{1}{\omega - \epsilon_{DQD}^{+} - \frac{\|T_+\|^2}{\omega-\epsilon_{M2}-\frac{\|T_-\|^2}{\epsilon_{DQD}^{-}}}}. \tag{A14}$$

From this analytical expression we can compute rapidly dynamical quantities such as the density of states in the non-interacting regime. Despite the difference this became a useful idea to predict interesting parameters for NRG simulation. Since the NRG code code takes about an hour to simulate each set of parameters in the Majorana-DQD mode, and even more if additional implementations are necessary, A14 became an important tool to improve our results.